JOURNAL OF SPACECRAFT AND ROCKETS
Vol. 37, No. 4, July–August 2000

Derivation of Atmospheric Gust-Forcing Functions for Launch-Vehicle Loads Analysis

B. H. Sako,* M. C. Kim,† A. M. Kabe,‡ and W. K. Yeung§
The Aerospace Corporation, Los Angeles, California 90009-2957

A methodology is developed to derive gust-forcing functions from the turbulent components of measured wind profiles. Several large sets of forcing functions were developed by extracting the short-duration, random component of measured Jimsphere wind profiles. A database consisting of Jimsphere wind soundings measured over the past three decades at the Eastern and Western Ranges of the United States was used to derive the forcing functions. Validity of these forcing functions for heavy-lift and medium-lift launch vehicles was established by examining the error contributions from various sources within the wind measurement system and the application of a noise-reducing filter. A unique aspect of the method is the extraction of the relatively rapidly changing turbulent component associated with the nonpersistent wind features, which are expected over a given observation time period. The gust-forcing functions can be used in a Monte Carlo analysis to determine launch-vehicle loads for the Eastern and Western Ranges.

Nomenclature

A = wind velocity amplitude, ft/s
AF_B = balloon's response amplification factor
AF_{Rose} = Rose program amplification factor
D_B = balloon's diameter, ft
f = wave number, cycles/ft
G = wind-speed power spectral density, $\text{ft}^3/\text{s}^2/\text{cycle}$
g = gravitational acceleration, ft/s^2
H_{opt} = optimal filter's frequency response
h = altitude, ft
L = balloon's lag distance, ft
L_{avg} = Rose program averaging layer length, ft
m_A = balloon's apparent mass, lb
m_B = balloon's mass, lb
m_0 = balloon's displaced mass, lb
n = wind measurement noise, ft/s
R = balloon's response distance, ft
Re = Reynolds number
U = wind velocity in the east–west direction, ft/s
V = wind velocity in the north–south direction, ft/s
W = one-dimensional wind field, ft/s
$\hat{W}$ = measured one-dimensional wind field, ft/s
W_X = wind field in the x direction, ft/s
$\dot{x}_B$ = balloon's horizontal velocity, ft/s
$\dot{z}_B$ = balloon's rise rate, ft/s
γ = wind's spectral density power law exponent
λ = vertical wavelength of horizontal wind field, ft
λ_B = wavelength defining the boundary between persistent and nonpersistent wind features, ft
λ_G = high-pass filter's corner wavelength used to extract turbulent wind features, ft
ν = kinematic viscosity of air, ft^2/s
ρ_A = ambient density of atmosphere, lb/ft^3
φ_B = balloon's phase response, rad
ω = atmospheric bouyancy frequency, cycles/s

Presented as Paper 99-1251 at the AIAA/ASME/ASCE/AHS/ASC 40th Structures, Structural Dynamics, and Materials Conference, St. Louis, MO, 12–15 April 1999; received 15 December 1999; revision received 14 April 2000; accepted for publication 18 April 2000.

*Senior Engineering Specialist, Structural Dynamics Department, P.O. Box 92957-M4/915. Member AIAA.
†Engineering Specialist, Structural Dynamics Department, P.O. Box 92957-M4/909. Member AIAA.
‡Director, Structural Dynamics Department, P.O. Box 92957-M4/911. Senior Member AIAA.
§Engineering Specialist, Structural Dynamics Department, P.O. Box 92957-M4/915.

Introduction

GUST loads analyses are performed to establish structural loads that a launch vehicle and its payload may experience as a result of atmospheric turbulence. Because these loads are driven by relatively rapidly changing wind features, gust loads must be determined statistically.

Current analysis procedures employ synthetic gust velocity profiles that are designed to yield loads of a desired level of statistical conservatism.[1] Typically, the analysis is performed by instantaneously enveloping the launch vehicle in the selected gust velocity profile. Parameters such as amplitude, shape, and wavelength of the synthetic gusts are selected to induce in the launch-vehicle/payload system a desired level of load. The most common waveform currently used is a one-minus cosine shape; on some vehicles a one-minus cosine with a flattop is used.[1] Other profiles have also been proposed.[2]

Work to date has concentrated on analysis of wind features to establish the shape and magnitude of the synthetic profiles, or to develop a statistical description of atmospheric turbulence.[3–14] However, none of these efforts has established the loads of launch vehicles subjected to actual short duration atmospheric turbulence. This paper will present a methodology that extracts the turbulent component from measured wind profiles to define empirical forcing functions that can be used in Monte Carlo gust loads analyses.[15] Several large sets of forcing functions were developed by extracting the short-duration, random component of measured Jimsphere wind profiles. A database consisting of over 1000 Western Range (WR) and over 1000 Eastern Range (ER) wind soundings, dating from 1964 to 1997, was used to derive the forcing functions.

Jimsphere-Radar System

Over the last several decades horizontal wind fields as a function of altitude have been measured in the United States at both the ER in Florida and the WR in California using radar-tracked Jimsphere balloons.

The Jimsphere is a 6.5-ft-diam, rigid spherical balloon constructed of 0.5-mil aluminized Mylar.[16] Rigidity is accomplished by maintaining an internal overpressure using valves 180 deg apart, which vent helium as the balloon rises. The balloon's surface is roughened by 398 conical elements to reduce both amplitude and spectral bandwidth of the lateral self-induced motions resulting from aerodynamic forces. A 0.22-lb ballast is added to lower the center of gravity in order to minimize spurious motions. The Jimsphere's ascent rate decreases almost linearly from 17.6 ft/s at 3.3 kft to

15.1 ft/s at 50 kft (Ref. 17). An AN/FPS-16, C-band, monopulse radar tracks the Jimsphere and provides position coordinates (slant range, azimuth, and elevation angles) at 0.1-s intervals.

Data reduction is performed by the Rose software program,[18] which processes the radar data to provide wind velocity as a function of altitude in 100-ft increments. Before transforming the data to Cartesian coordinates, the Rose program edits the radar data for outliers by monitoring the standard deviation of the first differences over 50-point segments. By computing a centered difference of the position vectors, which are averaged over 50-ft bands, wind velocity at 100-ft increments is established. This effective 100-ft averaging layer remains constant under light wind conditions when radar tracking is good. However, as the quality of the radar track deteriorates, as indicated by the standard deviation of the balloon's rise rate, Rose attempts to maintain an accuracy to about 3 ft/s by increasing the averaging layer in increments of 100 ft up to a maximum of 400 ft (Ref. 18).

Accuracy of Wind Profiles

The validity of turbulence/gust-forcing functions derived from measured wind profiles is directly related to the accuracy of the measured wind profiles. Accuracy of the Jimsphere-Radar system in measuring horizontal wind velocity has been investigated by a number of authors. Zartarian and Thompson[19] provided detail comparisons between balloon/radar systems and between data reduction methods in terms of wind profile accuracy. Luers and MacArthur[20] investigated the effects of variable rise rates on wind error magnitudes. Recently, Ref. 18 discussed how the effective vertical resolution is limited by radar noise and the self-induced oscillation. We shall examine the main sources of errors in the measurement system and how they affect the vertical resolution of wind profiles.

Amplitude and Phase Response

The planar equations of motion for an ascending balloon are discussed in Refs. 16 and 19. With some simplifying assumptions—lift forces are absent and the vertical wind component is zero—one can show that the balloon's steady-state horizontal velocity $\dot{x}_B$ when subjected to a sinusoidal wind field defined by

$$W_x = A \sin[(2\pi/\lambda)\dot{z}_B t] \tag{1}$$

is given by

$$\dot{x}_B = AF_B \cdot A \sin[(2\pi/\lambda)\dot{z}_B t - \varphi_B] \tag{2}$$

The following expressions for AF_B and φ_B were derived by Eckstrom[21]:

$$AF_B = \sqrt{\left(1 - \frac{(L/R)(2\pi R/\lambda)^2}{1 + (2\pi R/\lambda)^2}\right)^2 + \left(\frac{(L/R)(2\pi R/\lambda)}{1 + (2\pi R/\lambda)^2}\right)^2} \tag{3}$$

$$\varphi_B = \tan^{-1}\left(\frac{(L/R)(2\pi R/\lambda)}{1 + [1 - L/R](2\pi R/\lambda)^2}\right) \tag{4}$$

where

$$L = m_B/(m_0 - m_B) \cdot \dot{z}_B^2 \big/ g$$

is the lag distance,

$$R = (m_B + m_A)/(m_0 - m_B) \cdot \dot{z}_B^2 \big/ g$$

is the response distance, and the displaced mass and apparent mass are defined by

$$m_0 = \rho_A(\pi/6)D^3$$

$$m_A = 0.51 m_0$$

Plots of AF_B and φ_B are shown in Fig. 1 for altitudes of 30 and 45 kft. Because the Rose program provides wind velocity at 100-ft increments, Shannon's Sampling Theorem (Ref. 22) implies that we are limited to wind features with wavelengths greater than 200 ft. From Fig. 1 we see that at these wavelengths the Jimsphere is able to follow the wind field with less than 5% attenuation.

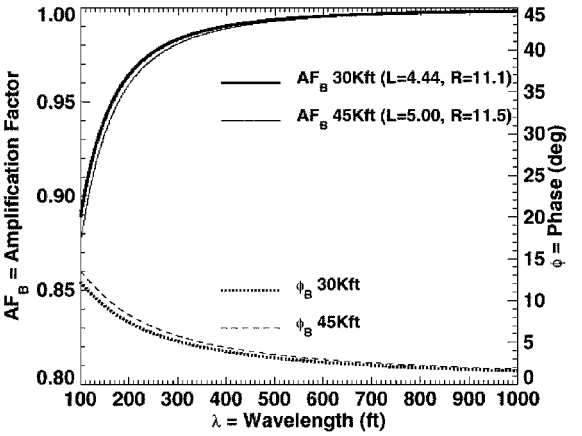

Fig. 1 Amplification factor and phase response plots for Jimsphere at 30 and 45 kft.

Rose Program Processing Effects

Errors introduced by the Rose program can be established following an analysis[23] that developed a least-squares smoothing technique for obtaining wind profiles from balloon sensor position coordinates. Assuming a sinusoidal horizontal wind field as defined by Eq. (1), Ref. 23 determined the distortion introduced by the smoothing procedure when applied to the balloon's position, given by

$$x_B = (\lambda/2\pi)(AF_B A)\cos[(2\pi/\lambda)h - \varphi_B] \tag{5}$$

where the altitude h is defined as

$$h = \dot{z}_B t$$

For simplicity we take φ_B to be zero and assume the rise rate $\dot{z}_B$ to be constant over the duration of interest. It is stated in Ref. 19 that the smoothing scheme, known as the University of Dayton Research Institute method, introduces no phase distortion, and for a given averaging layer L_{avg} attenuates the velocity amplitude by the amplification factor

$$AF_{\text{Rose}} = \text{sinc}^2(L_{\text{avg}}\pi/2\lambda) \tag{6}$$

where the sinc function is defined by

$$\text{sinc}(x) \equiv \sin(x)/x$$

We shall derive the preceding expression. Averaging x_B over half of the averaging layer, we see that its mean position is given by

$$\bar{x}_B(h) = \frac{2}{L_{\text{avg}}}\int_{h - L_{\text{avg}}/4}^{h + L_{\text{avg}}/4} x_B(h')\,\mathrm{d}h'$$

$$= \text{sinc}\left(\frac{L_{\text{avg}}\pi}{2\lambda}\right) \cdot x_B(h) \tag{7}$$

Applying a central difference to Eq. (7) using $\bar{x}_B(h \pm L_{\text{avg}}/2)$ leads to the following expression for the estimation of the balloon's velocity:

$$(\dot{x}_B)_{\text{Rose Estimate}} = \text{sinc}^2(L_{\text{avg}}\pi/2\lambda) \cdot (AF_B A)\sin[(2\pi/\lambda)h] \tag{8}$$

By comparing Eq. (8) with Eq. (2), we see that Rose introduces no phase shift and attenuates the velocity amplitudes by the factor defined in Eq. (6). Figure 2a presents plots of the preceding, using averaging layers of 100, 200, 300, and 400 ft, respectively. Observe that under nominal tracking conditions the 100-ft averaging layer causes less than 5% attenuation at wavelengths greater than 500 ft. Earlier implementation of the Rose program used an averaging layer and altitude increments of 82 ft (Ref. 19).

To verify Eq. (6), the Rose program was acquired, and simulated radar data measuring sinusoidal wind profiles of known wavelengths were processed. The nominal averaging layer of 100 ft and a rise rate $\dot{z}_B = 15.6$ ft/s corresponding to an altitude of 35 kft were used.

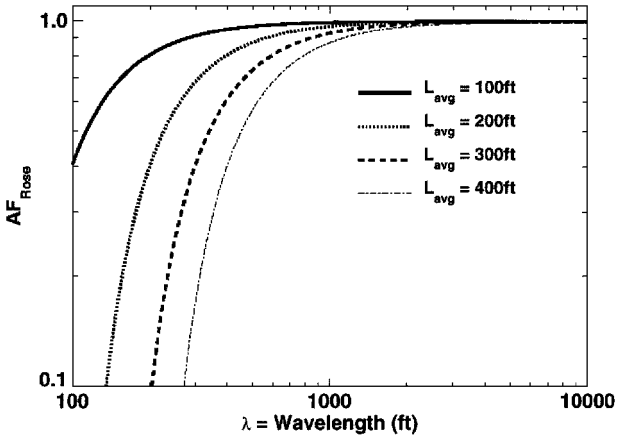

Fig. 2a AF_{Rose} at various averaging layer lengths.

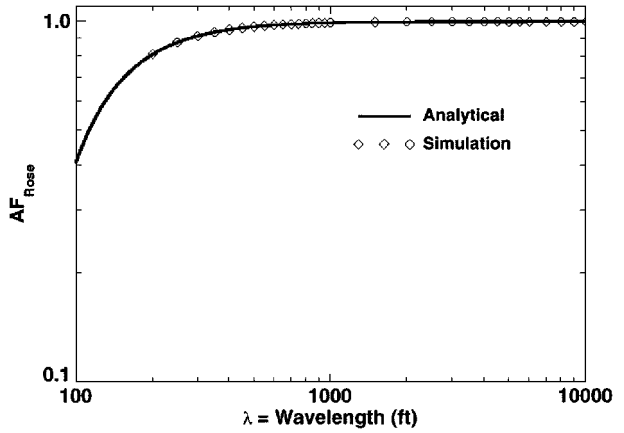

Fig. 2b Comparison of attenuation factors from Rose program simulations.

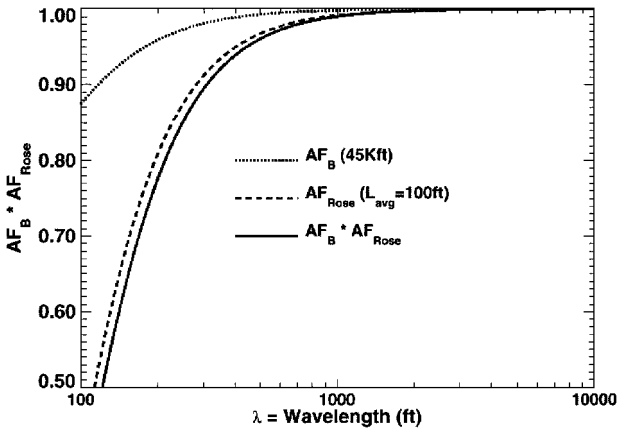

Fig. 3 Combined amplification factor from Jimsphere and Rose program.

The simulated results are shown in Fig. 2b, which agree well with the analytical expression just presented.

The extent to which the Jimsphere's response characteristics and the Rose program's smoothing scheme distort the true wind velocity can now be quantified for wavelengths greater than 500 ft. Because Rose introduces no phase shifts, we have from the preceding discussion that phase distortion is less than 1%, all of which is produced by the balloon's ability to follow the wind. Whereas phase is additive, amplification factors are multiplicative, therefore implying that the product $AF_B \cdot AF_{\text{Rose}}$ indicates the combined attenuation effects of the balloon's dynamics and the data reduction method. Figure 3 shows that, for the nominal averaging layer of 100 ft, the combined attenuation effect of the Jimsphere and the Rose program is less than 5% at wavelengths greater than 500 ft.

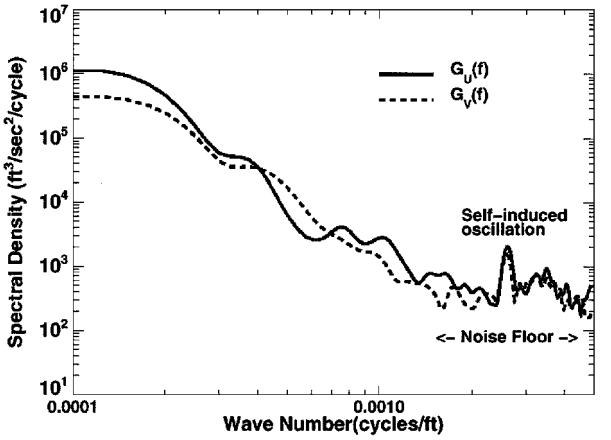

Fig. 4 Power spectral density of a Jimsphere wind profile with a strong self-induced oscillation.

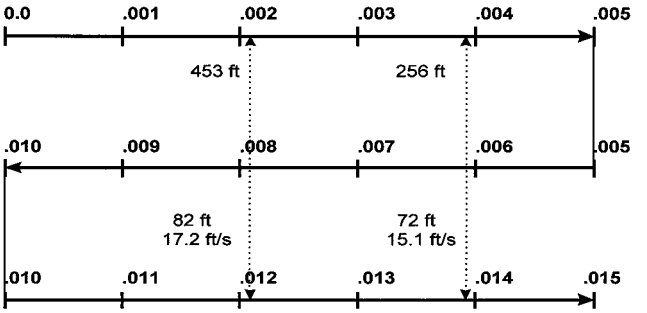

Fig. 5 Nyquist folding diagram showing the aliasing of the self-induced oscillations.

Self-Induced Oscillations and Aliasing Errors

It is well known[19,24] that the Jimsphere will exhibit lateral self-induced motion caused by aerodynamic lift forces that depend on the Reynolds number

$$Re = |\dot{z}_B| D_B / \nu$$

At a subcritical Reynolds number, i.e., $Re \leq 2.5 \times 10^5$, which occurs at altitudes greater than 35 kft, the Jimsphere will execute a regular 0.21-Hz spiral motion.[24] Unlike smooth balloon sensors whose lateral motions become erratic at supercritical Reynolds numbers $Re > 2.5 \times 10^5$, the roughness elements of the Jimsphere allow it to maintain its spiral motion throughout its ascent.

Reference 24 determined that the velocity's amplitude was proportional to $\dot{z}_B$ and that it decreased linearly with altitude from 7.9 ft/s near the surface to 3.3 ft/s at 49 kft. The Rose program does not remove the effects of the self-induced oscillations. Therefore, because of aliasing, this oscillation would manifest itself as oscillations with wavelengths in the neighborhood of 300 ft. Figure 4 shows the power spectral density (PSD) function of an atypical Jimsphere wind profile with a strong spectral peak caused by the self-induced oscillations. A 0.21-Hz oscillation implies that the Jimsphere completes one cycle every 4.76 s. Therefore, the variation in the Jimsphere's rise rate corresponds to variations in wavelengths of about 82 ft near the surface to 72 ft at 50 kft. Figure 5 shows how the Rose 100-ft sampling aliases these to wavelengths between 450–250 ft. Reference 18 verified the effects of aliasing and quantified these errors by applying the Rose program to radar data for simulated balloon releases. With the nominal averaging layer of 100 ft, their results indicate aliasing errors of 1.5 ft/s at 15 kft decreasing almost linearly to 0.15 ft/s at 50 kft.

Radar Errors

The performance of the AN/FPS-16 radar in tracking the Jimsphere has been examined by a number of investigators.[19,25–27] Basically, radar errors are classified as either bias errors or noise errors. In general, bias errors do not contribute significantly to wind

measurement errors because they are effectively removed by the central differencing done within the Rose program. On the other hand, noise error in position persists into the velocity estimate, which produces a noise floor in the wind's PSD (Fig. 4).

Using 33 dual-tracked Jimspheres, Ref. 18 computed the rms vector difference, which was then scaled by $1/\sqrt{2}$ to account for the noise contributions from the two radars. The result indicates that the radar noise error increases with slant range, typically ranging from 1 ft/s at low altitudes to 2 ft/s above 45 kft. Additionally, Ref. 18 concluded that the wavelength at which the noise floor becomes apparent effectively limits vertical resolution to approximately 500–650 ft under good tracking conditions and 800–1000 ft at longer slant ranges.

Validity of Wind-Derived Forcing Functions

From the preceding discussion it is reasonable to conclude that the Jimsphere wind profiles at the altitudes of interest (30–50 kft) for this study contain accurate wind velocity data at wavelengths longer than 500 ft. At these wavelengths the attenuation and phase errors introduced by the Jimsphere's response characteristics and the Rose program are small. Although aliasing of the self-induced oscillations limits the accuracy of the wind to wavelengths larger than 500 ft, these errors are reduced at the higher altitudes of interest to less than 1 ft/s.

Perhaps the greatest source of error, which degrades the accuracy of measurements, is radar noise. In general, these errors limit effective vertical resolution to approximately 500 ft. However, under inclement weather, where tracking conditions are poor, radar noise will contaminate wind features at scales as large as 1000 ft with RMS errors of about 2 ft/s. For these measurements we shall show that a simple noise-reducing filter extends the usable spectrum to include wind features as small as 500 ft.

The accuracy in measured winds, therefore, makes turbulence/gust-forcing functions derived from these wind profiles applicable to loads analyses of launch vehicles whose lower modes of vibration correspond to wavelengths longer than 500 ft. Currently, launch vehicles that are classified as medium-lift launch vehicles (MLV) and heavy-lift launch vehicles fall into this category. The forcing functions derived here should not be used on systems whose critical loads are defined by the shorter wavelength components of atmospheric turbulence, i.e., less than 500 ft. Many small launch vehicles and most space vehicles fall into this category.

Wind Database Description

A database consisting of 1093 WR and 1197 ER Jimsphere wind profiles dating from 1964 to 1997 was used in the derivation of the forcing functions. Most of the wind data collected during this period were associated with day-of-launch operations. Figure 6 shows the monthly distributions of the wind profiles. As mentioned earlier, some of the Jimsphere wind radar data were reduced, using an averaging layer and altitude increment of 82 ft, rather than the current

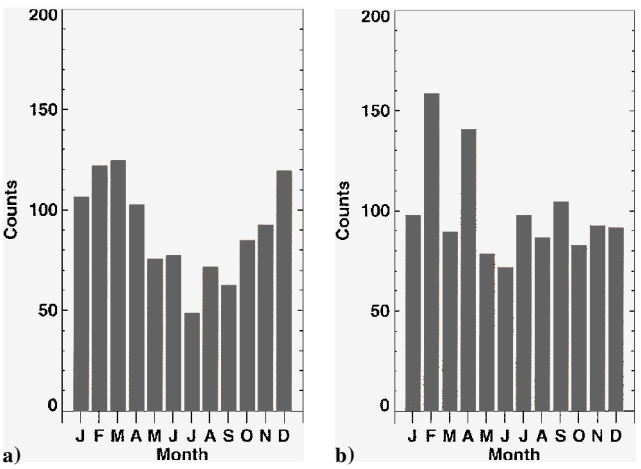

Fig. 6 Monthly distributions of a) WR and b) ER Jimsphere wind profiles.

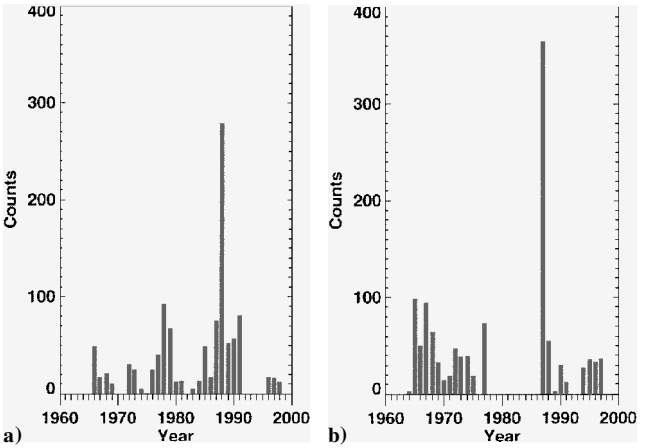

Fig. 7 Yearly distributions of Jimsphere wind profiles for a) WR and b) ER.

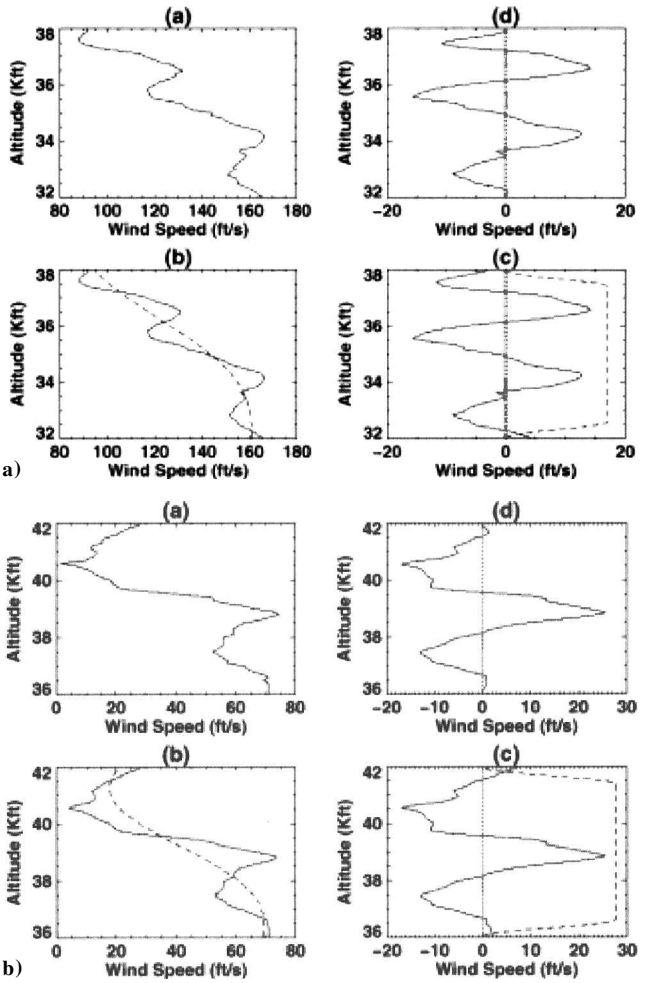

Fig. 8 Two examples of the method used to derive forcing functions: a) unfiltered wind magnitude at 32–38 kft; b) two-point smoothing denoising and high-pass filter detrending; c) tapering of the filtered wind profile; and d) resulting turbulent wind component to be used in launch-vehicle gust loads analysis.

standard of 100 ft. In general, WR winds prior to 1989 and ER winds prior to 1987 were processed using 82 ft. The yearly distributions are shown in Fig. 7.

Forcing Functions Derivation

Figure 8 illustrates the process used to derive forcing functions from two wind profiles. Figure 8a shows a sample wind magnitude profile restricted to the 32–38-kft-altitude band. A moving two-point average was applied to remove the noise floor. In Fig. 8b, shown by the dashed line, is the trend that the high-pass filtering removed to

yield the small-scale and rapidly changing wind features. Figure 8c shows the flattop tapering performed on the resulting filtered data to minimize step response transients. The final turbulent component of the wind to be used as the forcing function is shown in Fig. 8d. The following subsections describe in further detail each of the preceding steps.

Removal of Noise Floor

Radar noise accounts for the leveling of the wind's PSD at wavelengths near 500–1000 ft. That this noise floor is not indicative of wind features is based on numerous investigations that show that despite seasonal, climatic, and topographical differences, the wind's vertical wave-number PSD obeys a power law of the form

$$G(f) \propto \omega^2 / f^{\gamma}$$

VanZandt[28] was the first to describe this, using $\gamma = 2.4$, in terms of a universal spectrum of atmospheric buoyancy waves.[29,30] References 29 and 30 modeled similar spectra observed in the ocean.

Dewan and Good[31] later conjectured that the PSD amplitudes at any given wave number are limited by its saturation value, likely caused by convective instability. Their theory leads to a PSD power law with $2.5 \leq \gamma \leq 3$. Moreover, they showed that simple dimensional analysis yields $\gamma = 3$ because the PSD should scale as $Hz^2/(cycles/ft)^3$. Reference 32 advanced a more general theory arguing that the spectral amplitude should decrease as $1/f^3$, resulting from the superposition of individually saturated gravity waves.

Further evidence that the noise floor is directly related to the radar noise is obtained from dual-tracking experiments.[18,33] Reference 18 computed cross-spectral densities (CSD) for 33 dual-tracked Jimsphere wind profiles. Their results showed that except for the presence of the aliased self-induced oscillation the CSD amplitudes conform to the power law and, moreover, confirmed the hypothesis that the noise floor is caused by radar noise, which is uncorrelated to the true wind profile.

Figure 9 shows that the ensemble averages of wind magnitude PSDs from WR and ER obey the power law with $\gamma \approx 2.7$. Each PSD was computed via the method described in Bendat and Piersol[34] using 10-kft discrete Fourier transforms, with 50% overlap, and a Hanning data window. The onset of the noise floor at wavelengths smaller than 500 ft implies that we can, in general, expect adequate resolution at this scale. Additionally, we note that WR's PSD is greater than that of ER, thereby implying that turbulence from WR tends to be more severe than ER.

Because the noise floor is not a measure of the wind, we need to minimize its contribution to the forcing functions by low-pass filtering. Another reason for minimizing the noise floor is to ensure that the Monte Carlo gust loads analysis approach is applicable to MLVs, which typically require wavelengths starting in the neighborhood of 800 ft. This requirement is generally met for light winds when radar tracking is good. Therefore, this concern applies mainly to the filtering of wind profiles, which were measured under strong wind conditions, when radar noise can corrupt wind components with wavelengths less than 1000 ft. The criterion for selecting a low-pass filter, therefore, was that it should remove the noise so that the resulting spectrum conforms to the power law.

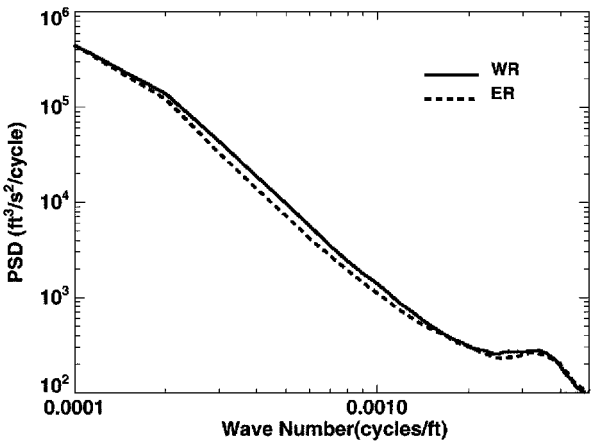

Fig. 9 Ensemble averages of wind magnitude PSDs from WR and ER.

An optimal filter (or Wiener filter) is generally used to remove noise from a waveform with a known PSD.[22,35] This approach was tried initially but later abandoned. The method assumes stationarity, and the true wind W is corrupted by uncorrelated noise n, thereby giving a measured wind of the form

$$\hat{W} = W + n$$

The optimal filter's frequency response could then be shown equal to

$$H_{\text{opt}}(f) = G_W(f) / G_{\hat{W}}(f)$$

where G_W and $G_{\hat{W}}$ are the PSDs corresponding to W and $\hat{W}$, respectively. Because G_W is unknown, it was replaced by a power law defined by a least-square fit over the interval $0.000125 \leq f \leq 0.00125$, leading to

$$H_{\text{opt}}(f) \approx C / f^{\gamma} / G_{\hat{W}}(f)$$

with C, a constant, defined by the fit. PSDs were computed for all WR and ER winds and the power law fitted to each spectrum. The resulting γ varied between 2 and 3.5 and depended upon the spectral estimation and the wave-number interval used for the fit. Moreover, it was found that, in general, these filters did not effectively remove the noise floor, and to do so required "tuning" each filter by increasing γ. Because of this lack of robustness, and the fact that each wind would have its own unique filter, another filtering scheme was sought.

The increase in γ, needed to remove the noise floor, indicates that a faster decay in the filter's amplitude response was needed. This led to considering filters having a zero at the Nyquist frequency. A two-point moving average, which averages consecutive data points, is the simplest of all finite-impulse-response filters with this property and was, therefore, selected for the purpose of removing the noise floor. Because wind profiles are reported at 100-ft increments, the resulting filtered data were also shifted forward by 50 ft to avoid any phase shifting.

Figure 10a shows a typical wind profile before and after filtering. The noise component, which was removed by the filtering procedure, is shown in Fig. 10b, which tends to increase with slant range, as does radar noise. Figure 11 compares the PSD of filtered and unfiltered data. The unfiltered data have a noise floor beginning at 1000 ft. We see that based on adherence to the power law this filtering scheme extends the usable spectrum to wavelengths as small as 500 ft. Also shown in Fig. 11 is the PSD of the noise component, which has the characteristic flat spectrum.

Extraction of Turbulent Wind Features

Extraction of the small-scale turbulent component of the wind was accomplished by way of a high-pass filter. For the gust-forcing functions the filter's corner wavelength λ_G was based on earlier work,[36] which analyzed hundreds of wind pairs and established a wavelength boundary λ_B, where wind features smaller than it no longer remain coherent after a given length of time. The component of the wind, which consisted of these small-scale and short-duration wind features, was referred to in Ref. 36 as the rapidly varying, turbulent component of the wind. Using wind pairs from the database, Ref. 36 estimated the mean wavelengths, which spectrally separate the slowly varying and turbulent wind components for wind pairs 30, 60, 90, and 120 min apart. A curve fit was then applied to this data that led to the simple empirical formula relating λ_B as a function of the time ΔT between wind pairs:

$$\lambda_B = 460 \sqrt{\Delta T}$$

The preceding formula suggests that as ΔT increases so does the lack of wind persistence at longer wavelengths, which needs to be

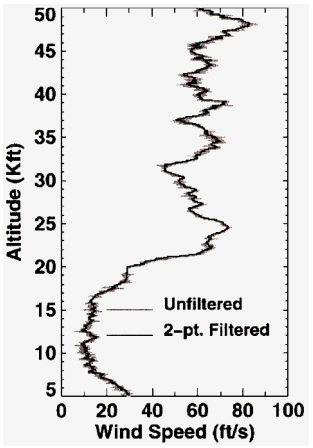

Fig. 10a Comparison of unfiltered and two-point filtered wind profile.

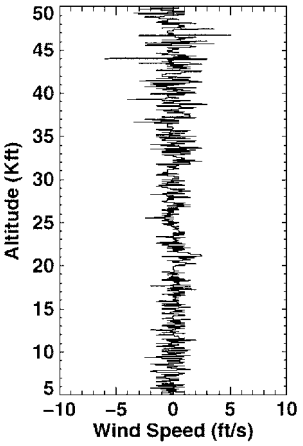

Fig. 10b Noise removed by the two-point filtering.

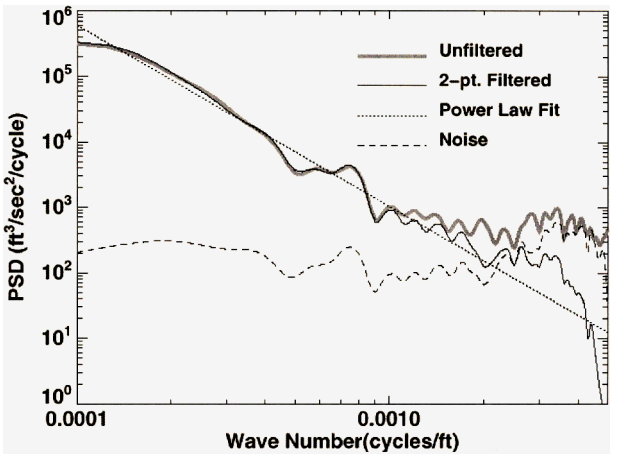

Fig. 11 PSD comparison of the two-point filtered profile, the noise it removes, and the power law.

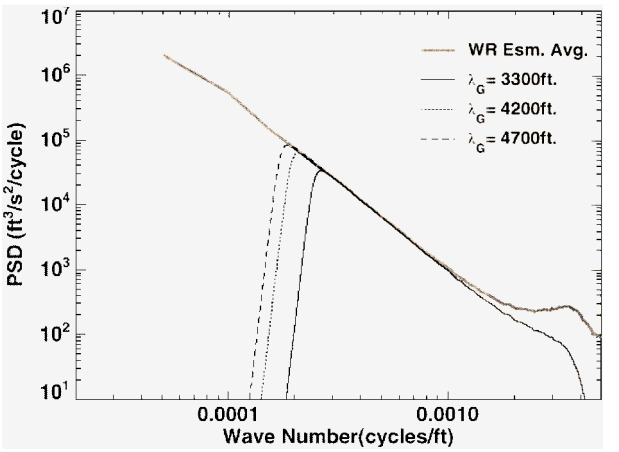

Fig. 12 Ensemble averages of filtered wind PSDs for $\lambda_G = 3300, 4200,$ and 4700 ft.

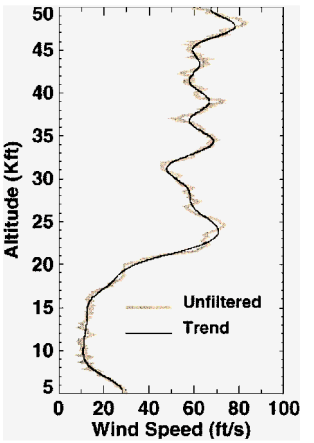

Fig. 13a Two-point smoothed wind and trend removed by the high-pass filter for λ_G = 3300 ft and ΔT = 30 min.

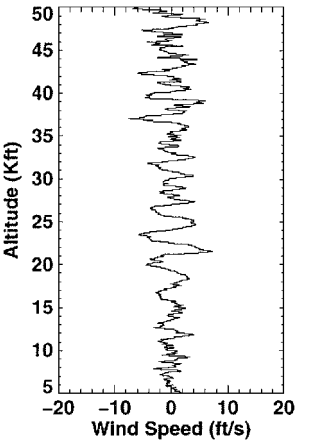

Fig. 13b Resulting filtered wind profile.

accounted for in a gust analysis. Because of the variation about the estimated λ_B, and to ensure sufficient conservatism in the forcing functions, λ_G was defined by λ_B plus an estimated one standard deviation, which also depended upon ΔT. For the purpose of this study, the standard deviations were estimated from the normal regions of the wavelength histograms presented in Ref. 36 and resulted in three-filter corner wavelengths, λ_G =3300, 4200, and 4700 ft, corresponding to ΔT of 30, 45, and 60 min, respectively.

A 16-pole Butterworth high-pass filter was applied where the filter's half-power cutoff frequency was selected so that the attenuation of wind features smaller than λ_G was less than 1%. Moreover, the high-pass filter was applied forward and then backward to eliminate phase shifts. This procedure was applied using the three-filter corner wavelengths λ_G.

The PSD curves shown in Fig. 12 illustrate, spectrally, the effect of the high-pass filtering on the wind profiles using the three-filter corner wavelengths. The corresponding effects of filtering in the altitude domain are shown in Figs. 13–15. In these examples the 2-pt smoothed wind magnitude profile shown in Fig. 10a was high-pass filtered at the corner frequencies just stated. The figures show how increases in the time ΔT, for which the forcing functions are valid, result in additional longer wavelength wind features in the gust-forcing functions.

Restriction to 6000-ft Bands

Because of the variation in the structural dynamic properties, aerodynamic characteristics, and the launch-vehicle's velocity, and the desire to have altitude consistent gust loads, the gust analysis[15] required each filtered wind profile to be restricted to an altitude band

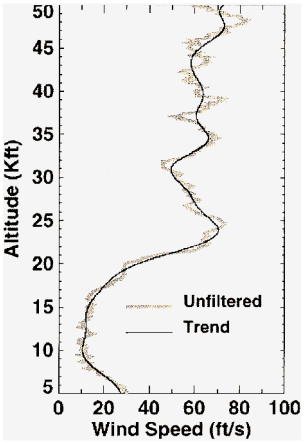

Fig. 14a Two-point smoothed wind and trend removed by the high-pass filter for $\lambda_G = 4200$ ft and $\Delta T = 45$ min.

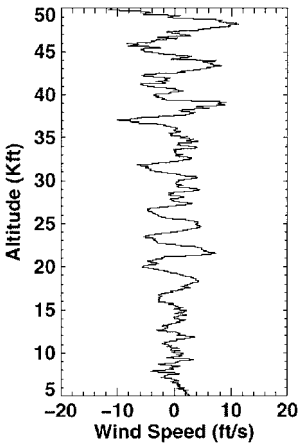

Fig. 14b Resulting filtered wind profile.

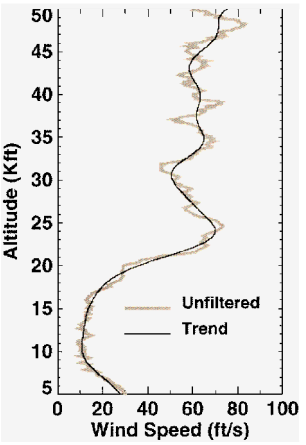

Fig. 15a Two-point smoothed wind and trend removed by the high-pass filter for $\lambda_G = 4700$ ft and $\Delta T = 60$ min.

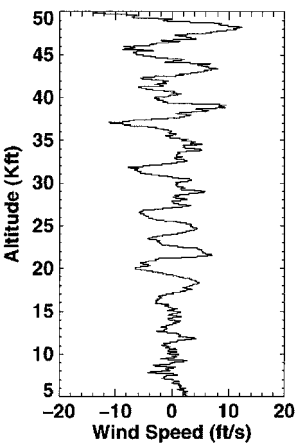

Fig. 15b Resulting filtered wind profile.

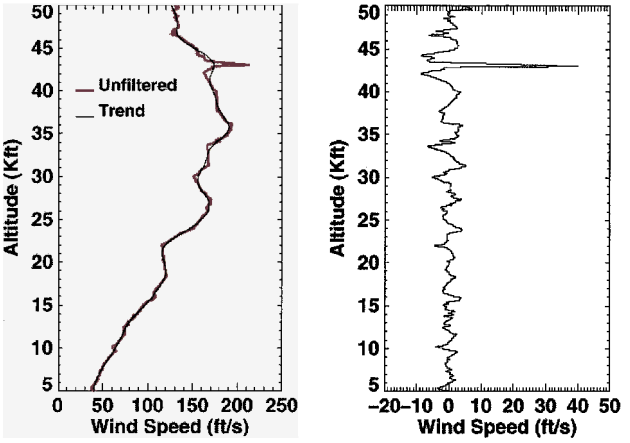

Fig. 16 Wind profile failing the shear criteria with $dW/dh|_{max} \approx 0.28\ s^{-1}$ and $\lambda_G = 3300$ ft.

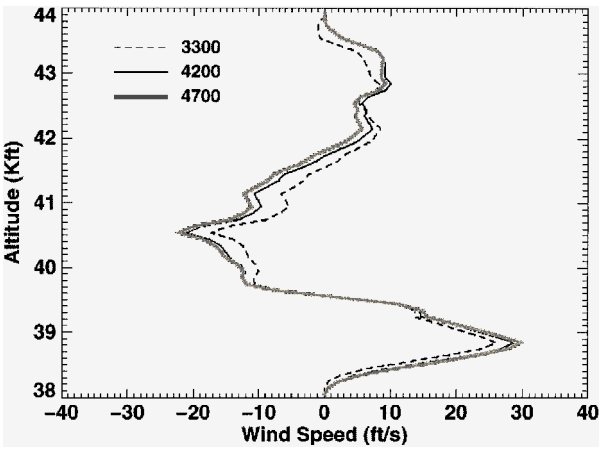

Fig. 17 Gust-forcing function comparisons using different λ_G. Taken from Jimsphere profile WR 02-12-72 08:59Z.

of 6000 ft. To minimize step responses during the gust loads simulations, a flattop window having a 10% cosine taper at each end was used (Fig. 8c). Turbulence/gust-forcing functions were developed for four overlapping 6000-ft bands covering an altitude range of 32–48 kft, i.e., 32–38-, 36–42-, 38–44-, and 42–48-kft-altitude bands. Thus, for each range λ_G and altitude band a total of 24 sets, each containing over 1000 forcing functions, was developed.

Screening of Wind Data Using a Shear Criterion

Most of the Jimsphere wind data were from day-of-launch balloons and hence have gone through some form of quality control. However, a few profiles exhibited questionable features and were generally associated with older data in which the data quality information was lost and, therefore, had to be either accepted or rejected based on engineering judgment.

The screening criterion selected was the wind-shear value. Wind shear is defined as dW/dh, where dW is the speed change for the altitude difference dh. A shear value greater than $0.1\ s^{-1}$ is unlikely. Generally, shear values from measured wind profiles that exceed $0.1\ s^{-1}$ are noise driven and are not caused by actual wind-shear features. If the high-frequency noise is removed, as was done by the 2-pt filtering, then it is unlikely that shears would exceed $0.1\ s^{-1}$. Therefore, the screening of wind data using a shear criterion of $0.1\ s^{-1}$ was used on the filtered winds. A typical wind profile that was rejected on this basis is shown in Fig. 16. Furthermore, each profile was visually reviewed to establish its reasonableness.

Results

Comparison plots of WR forcing functions, which were derived using various λ_G values, are shown in Figs. 17–19 for three

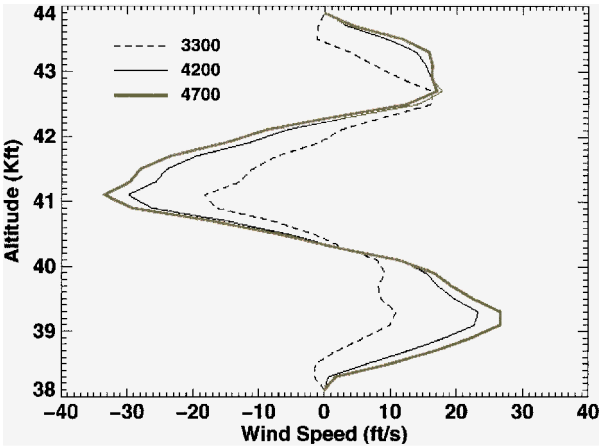

Fig. 18 Gust-forcing function comparisons using different λ_G. Taken from Jimsphere profile WR 10-12-78 03:45Z.

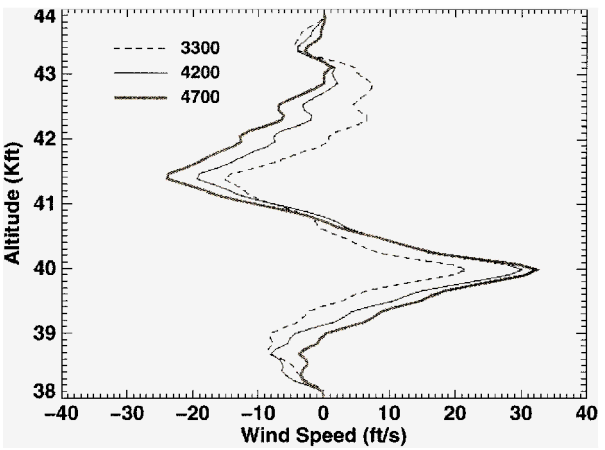

Fig. 19 Gust-forcing function comparisons using different λ_G. Taken from Jimsphere profile WR 05-02-88 19:00Z.

representative profiles. These figures indicate that there is a wide variation in forcing function profiles, which do not resemble the synthetic profiles used in past gust analyses.

The methodology described here was implemented in a computer program that generates a set of gust-forcing functions from the wind database for a given launch range, filter corner wavelength λ_G, and altitude band. The program was used to develop 24 sets of forcing functions that were used in the Monte Carlo gust analysis described in Ref. 15.

The primary purpose of this study was to establish the feasibility of deriving from measured wind profiles the turbulent component for use in launch-vehicle gust loads analyses. As such, the forcing functions were developed from the total magnitude of the wind. The procedures, as presented here, are applicable to deriving pairs of north–south and east–west forcing functions that can be applied to a launch vehicle simultaneously.

The forcing functions derived in this paper should not be applied simultaneously to the pitch and yaw planes of a launch vehicle. Moreover, the results of the individual pitch and yaw plane analyses should not be combined without accounting for the fact that each analysis was performed with the total wind turbulence.

Conclusions

A methodology for deriving forcing functions from Jimsphere wind profiles that can be used in Monte Carlo gust analyses was presented. Validity of these forcing functions for the wavelengths of interest was established by examining the error contributions from various sources within the wind measurement system and the application of a noise-reducing filter. A unique aspect of the method is the extraction of the relatively rapidly changing turbulent component of measured wind profiles.

Acknowledgments

The authors are grateful to Richard L. Walterscheid for his helpful comments and suggestions and to Timothy L. Wilfong for providing a version of the Rose program.

References

[1]Kabe, A. M., "Design and Verification of Launch and Space Vehicle Structures," AIAA Paper 98-1718, April 1998.

[2]Smith, S. A., "Revised Gust Model," NASA ES44-(147-89), Oct. 1989.

[3]Smith, O. E., and Adelfang, S. I., "On the Relationship Between Wind Profiles and the STS Ascent Structural Loads," AIAA Paper 89-0709, Jan. 1989.

[4]Daniels, G. E., "Natural Environment (Climatic) Criteria Guidelines for Use in MSFC Launch Vehicle Development," NASA MTP-AERO-63-8, Revision, Jan. 1963.

[5]Smith, O. E., Adelfang, S. I., and Batts, G., "Wind Models for the NSTS Ascent Trajectory Biasing for Wind Load Alleviation," AIAA Paper 90-0481, Jan. 1990.

[6]Haering, E. A., Jr., "Air Data Calibration Techniques for Measuring Atmospheric Wind Profiles," *Journal of Aircraft*, Vol. 29, No. 4, 1992, pp. 632–639.

[7]Johnson, D. L. (ed.), "Terrestrial Environment (Climatic) Criteria Guidelines for Use in Aerospace Vehicle Development," NASA TM 4511, Revision, Aug. 1993.

[8]Johnson, D. L. (ed.), "National Aerospace Plane (NASP) X-30 Natural Environment Requirements Document (Rev. 1.0)," NASP-NEC-NERD 031594, March 1994.

[9]de Jonge, J. B., "Reduction of Incremental Load Factor Acceleration Data to Gust Statistics," Rept. DOT/FAA/CT-94/57, Aug. 1994.

[10]Johnson, D. L., "Wind Gust Procedure for Shuttle Ascent," NASA EL23(13-97), 25 March 1997.

[11]Adelfang, S. I., and Smith, O. E., "Analysis of Extreme Wind Shear," AIAA Paper 89-0710, Jan. 1989.

[12]Adelfang, S. I., and Smith, O. E., "Analysis of Wind Perturbation Activity for the NSTS Launches," AIAA Paper 90-0482, Jan. 1990.

[13]Van Gelder, P. A., "Derivation of Lateral and Vertical Gust Statistics from In-Flight Measurements," AIAA Paper 97-1214, 1997.

[14]Adelfang, S. I., and Smith, O. E., "Gust Models for Launch Vehicle Ascent," AIAA Paper 98-0747, Jan. 1998.

[15]Kim, M. C., Kabe, A. M., and Lee, S. S., "Atmospheric Flight Gust Loads Analysis," *Journal of Spacecraft and Rockets*, Vol. 37, No. 4, 2000, pp. 446–452.

[16]Fichtl, G. H., "The Response of Rising or Falling Spherical Wind Sensors to Atmospheric Wind Perturbations," *Journal of Applied Meteorology*, Vol. 10, No. 6, 1971, pp. 1275–1284.

[17]DeMandel, R. E., and Krivo, S. J., "Radar/Balloon Measurement of Vertical Air Motions Between the Surface and 15 km," *Journal of Applied Meteorology*, Vol. 10, April 1971, pp. 313–319.

[18]Wilfong, T., Smith, S., and Crosiar, C., "Characteristics of High-Resolution Wind Profiles Derived from Radar-Tracked Jimspheres and the Rose Processing Program," *Journal of Atmospheric and Oceanic Technology*, Vol. 14, April 1997, pp. 318–325.

[19]Zartarian, G., and Thompson, J. H., "Validity of Detailed Balloon Soundings in Booster Vehicle Design," Air Force Cambridge Research Lab., Kaman Science Corp., AFCRL-68-0606, Burlington, MA, Oct. 1968.

[20]Luers, J. K., and MacArthur, C. D., "Ultimate Wind Sensing Capabilities of the Jimsphere and Other Rising Balloon Systems, NASA CR-2048, June 1972.

[21]Eckstrom, C. V., "Theoretical Study and Engineering Development of Jimsphere Wind Sensor, Final Report on Jimsphere Wind Sensor," Final Rept. on Contract NASA-11158, July 1965.

[22]Papoulis, A., *Signal Analysis*, 1st ed., McGraw–Hill, New York, 1977, pp. 336–339.

[23]Luers, J., and Engler, N., "On Optimum Methods for Obtaining Wind Data from Balloon Sensors," *Journal of Applied Meteorology*, Vol. 6, Oct. 1967, pp. 816–823.

[24]Fichtl, G. H., DeMandel, R. E., and Krivo, S. J., "Aerodynamic Properties of Spherical Balloon Wind Sensors," *Journal of Applied Meteorology*, Vol. 11, April 1972, pp. 472–481.

[25]Scoggins, J. R., and Susko, M., "FPS-16 Radar/Jimsphere Wind Data Measured at the Eastern Test Range," NASA TM X-53290, July 1965.

[26]Engler, N. A., Luers, J. K., and McCloskey, J. W., "An Analysis of the AN/FPS-16 Rose System," Air Force Cambridge Research Lab., Univ. of Dayton Research Inst., AFCRL-67-0534, Dayton, OH, Nov. 1967.

[27]Engler, N. A., Luers, J. K., McCloskey, J. W., and Strange, J. D., "Tracking Errors in Detailed Wind Soundings," Air Force Cambridge Research Lab., Univ. of Dayton Research Inst., AFCRL-69-0213, Dayton, OH, April 1969.

[28]VanZandt, T., "A Universal Spectrum of Bouyancy Waves in the Atmosphere," *Geophysical Research Letters*, Vol. 9, No. 5, 1982, pp. 575–578.

[29]Garrett, C., and Munk, W., "Space-Time Scales of Internal Waves," *Geophysical Fluid Dynamics*, Vol. 2, June 1972, pp. 225–264.

[30]Garrett, C., and Munk, W., "Space-Time Scales of Internal Waves: A Progress Report," *Journal of Geophysical Research*, Vol. 80, No. 3, 1975, pp. 291–297.

[31]Dewan, E. M., and Good, R. E., "Saturation and the 'Universal' Spectrum for Vertical Profiles of Horizontal Scalar Winds in the Atmosphere," *Journal of Geophysical Research*, Vol. 91, No. D2, 1986, pp. 2742–2748.

[32]Smith, S., Fritts, D., and VanZandt, T., "Evidence for a Saturated Spectrum of Atmospheric Gravity Waves," *Journal of Atmospheric Sciences*, Vol. 44, No. 10, 1987, pp. 1404–1410.

[33]Susko, M., and Vaughan, W. W., "Accuracy of Wind Data Obtained by Tracking Jimsphere Wind Sensor Simultaneously with Two FPS-16 Radars," NASA TM X-53752, July 1968.

[34]Bendat, J. S., and Piersol, A. G., *Random Data Analysis and Measurement Procedures*, 2nd ed., Wiley-Interscience, New York, 1986, pp. 391–400.

[35]Press, W. H., Flannery, B. P., Teukolsky, S. A., and Vetterling, W. T., *Numerical Recipes*, 1st ed., Cambridge Univ. Press, New York, 1986, pp. 417–420.

[36]Spiekermann, C. E., Sako, B. H., and Kabe, A. M., "Identifying Slowly Varying and Turbulent Wind Features for Flight Loads Analyses," *Journal of Spacecraft and Rockets*, Vol. 37, No. 4, 2000, pp. 426–433.

A. M. Kabe
Guest Editor